

Patterned backgating using single-sided mask aligners: application to density-matched electron-hole bilayers

A.F. Croxall, K. Das Gupta,* C.A.Nicoll, M. Thangaraj, I. Farrer, D. A. Ritchie, and M. Pepper
Cavendish Laboratory, University of Cambridge, J.J. Thomson Avenue, Cambridge CB3 0HE, UK.

We report our work on fabricating lithographically aligned patterned backgates on thin ($50-60\mu\text{m}$) III-V semiconductor samples using *single sided mask aligners only*. Along with this we also present a way to photograph both sides of a thin patterned chip using inexpensive infra-red light emitting diodes (LED) and an inexpensive (consumer) digital camera. A robust method of contacting both sides of a sample using an ultrasonic bonder is described. In addition we present a mathematical model to analyse the variation of the electrochemical potential through the doped layers and heterojunctions that are normally present in most GaAs based devices. We utilise the technique and the estimates from our model to fabricate an electron-hole bilayer device in which each layer is separately contacted and has tunable densities. The electron and hole layers are separated by barriers either 25 or 15nm wide. In both cases, the densities can be matched by using appropriate bias voltages.

Keywords: patterned backgate, double side alignment, electron-hole, bilayer

I. INTRODUCTION

Patterned backgating is a critical step in the processing of a large class of devices that use double quantum well structures,[1] or where manipulation of the shape and position of the wavefunction at a heterointerface is envisaged [2]. It is also of importance in devices where the top surface needs to remain non-metallised for STM/AFM or optical studies [3]. Investigation of surface states of semiconductors also requires a metal-free top surface, with a backgate to change densities when required[4]. Backgates can be either lithographically aligned to topside features using mask-aligners with double (bottom) side alignment capability or patterned in-situ during wafer-growth by using Focused Ion-Beam (FIB) techniques. [5] Both these solutions require complex and very expensive additional equipment. In this paper we present a technique of reproducible thinning of the sample (wet etching to $50\mu\text{m}$) and lithographically aligning a backgate with any existing topside features using a single sided mask-aligner at all stages. Conventional ultrasonic ball bonders can be used to contact gates on either side of the sample. Additionally, the alignment can be verified and photographed using inexpensive infra-red (IR) (wavelength 880/950nm) LEDs and a standard inspection microscope fitted with a digital camera. We have used this technique to study a 2-dimensional hole gas at an inverted GaAs/AlGaAs interface and independently contacted electron-hole bilayers in a double quantum well structure, however our technique can be easily adapted for use with almost any other material. Other techniques of fabricating lithographically patterned backgates (*e.g.* EBASE: Epoxy Bond and Stop Etch)[6] exist - however the utility of the technique presented here lies in the fact that a commonly available single-sided mask aligner can

be used at all stages.

The spatial variation of the bandstructure and the electrochemical potential near an interface must be analysed before attempting to change charge densities by backgating. We have used a self-consistent Poisson-Schrödinger-current equation solver [7] to analyse the variation of the Fermi-level under biasing and doping to estimate acceptable dopant densities without causing pinning of the Fermi-level and undesirable hopping conduction. Wafers were grown using these estimates as a guide and the patterned backgating method described in the next section was applied to fabricate independently contacted electron-hole bilayer devices with narrow barriers of the order of excitonic Bohr radius of GaAs ($\approx 12\text{ nm}$).

II. METHOD

In our design each chip contains a few crosshair shaped alignment marks on the topside at the centre and near the edges (see fig 1). The wafers are originally $500\mu\text{m}$ thick. On completion of topside processing the chips are mounted topside down on a thin glass slide with a transparent wax (CrystalbondTM 509 from SPI technologies) The wax melts at around 130°C , is resistant to the acid peroxide etch solution used, but would dissolve in acetone if soaked for a few hours. Using a diamond tipped mechanical scribe, the (crosshair shaped) alignment mark is then copied and extended onto the other side of the glass slide. It is for this step that the transparency of the wax is crucial. The fine groove ($\sim 5\mu\text{m}$ width) made on the glass are visible from both sides in regions not covered by the chip. Thinning of the chip is then carried out using an acid-peroxide (1:1:8 $\text{H}_2\text{SO}_4 : \text{H}_2\text{O} : \text{H}_2\text{O}_2$) solution with 2000:1 Triton-X surfactant (5ml per 50ml of etch solution). The solution is continuously agitated with a magnetic stirrer during the process. After an estimated time the chips are taken out and the thicknesses of the chips are measured with a step profilometer. The

*Electronic address: kd241@cam.ac.uk

process is continued until the chips are 50-60 μm thick. Lithography for the backgate layer is then done using the extended grooves on the glass as alignment marks, and a single sided mask aligner. The alignment can be verified before metallisation, using an inspection microscope fitted with a digital camera. To view both sides of the chip simultaneously we need radiation of a frequency to which a GaAs wafer is transparent. This is very easily provided by an infra-red LED (880/950nm) placed below the microscope stage. Since the CCD sensors used by all digital cameras have a finite sensitivity to IR, the camera sees both surfaces of the chip simultaneously (see fig1,2) The strength of the IR illumination from the bottom and visible light from the top are adjusted to get a picture with good clarity of both sides. After the back-

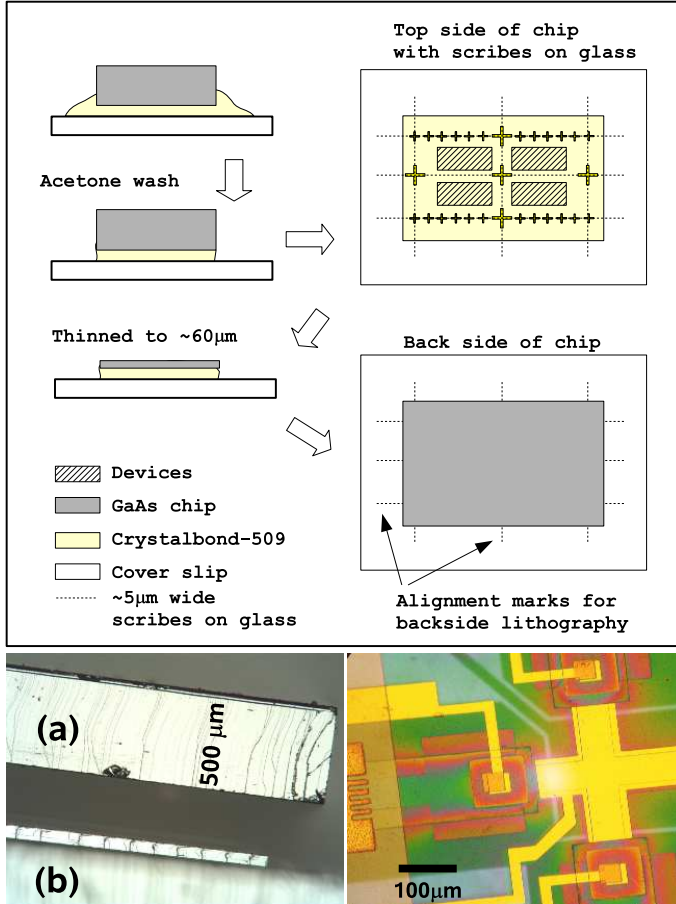


FIG. 1: (Color online) Top: Figure illustrates the processing steps for doing backside lithography. Bottom left: typical cross-section of a device before (a) and after (b) thinning to <60 μm . Bottom right: Infra-red+visible composite photograph of a processed device, taken using the method described in the section, showing the alignment accuracy (better than ~5 μm) that can be obtained.

gate metallisation is done the individual devices can be diced while the chips are still fixed on the glass. Finally a long soak in acetone is used to dissolve away the Crystalbond wax. The individual devices are then mounted on

a piece of pre-patterned semi-insulating GaAs substrate. This substrate has 20 μm deep channels etched and metallised to match the contact pads on the backgate side of the device. Once the thinned device is positioned on the substrate, small drops of silver epoxy are placed on these channels. The epoxy flows along the channels and contacts the underside of the chip in specific places. Once it is cured it provides electrical contact as well as mechanical support to the thinned device. Gold-wire bonds can then be made to the contact pads on the topside and to the extensions of the backgates provided by the conducting epoxy.

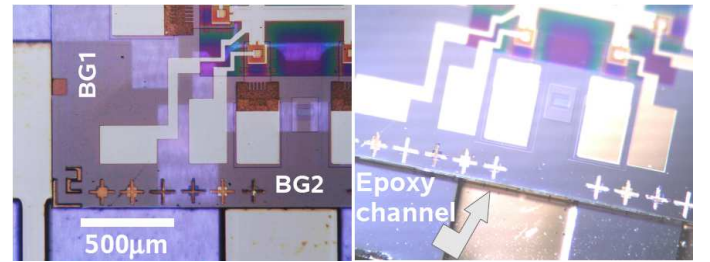


FIG. 2: (Color online) Mounting of sample for bonding to backgates. Left: Alignment of the backgate with etched channels. Right: The etched channels for contacting the backgates are about ~20 μm deep and would be filled with a small amount of Silver-epoxy.

III. A SELF-CONSISTENT MODEL OF GATE ACTION

Techniques for calculating the band-bending and carrier densities in layered heterostructures are well known. We review the procedure very briefly. Normally a self-consistent solution of Poisson's equation and the Schrödinger equation (for the envelop function) is calculated[8]. Poisson's equation relates the electrostatic potential ($\phi(x)$) to the total charge density $\rho(x)$

$$\nabla \epsilon(x) \nabla \phi(x) = -\rho(x) \quad (1)$$

The envelope function (ψ) is determined by the Schrödinger equation :

$$-\frac{\hbar^2}{2} \frac{d}{dx} \left(\frac{1}{m^*} \frac{d}{dx} \right) \psi_j(x) + V(x) \psi_j(x) = E \psi_j(x) \quad (2)$$

Where $V(x) = |e|\phi(x) + \Delta E_c(x)$, the potential confining the electrons is the sum of the electrostatic potential and the conduction band offset at the heterointerface. $\epsilon(x)$ is the position dependent dielectric constant, E_j and ψ_j are the subband energies and envelope functions that solve equation 2. The charge density at each point is given by the sum of the localised charge ($N_D^+(x)$) on the ionised donors (or acceptors) and the electron (hole) densities ($n(x)$) in the conduction (valence) band. E_D denotes the donor energy level.

$$\rho(x) = |e|N_D^+(x) - |e|n(x) \quad (3)$$

$$N_D^+(x) = \frac{N_D(x)}{1 + \frac{1}{2} \exp(\frac{E_f - E_D}{kT})} \quad (4)$$

$$n(x) = \sum_j |\psi_j(x)|^2 \frac{m^*}{\pi \hbar^2} \int_{E_j}^{\infty} \frac{dE}{1 + \exp \frac{E - E_f}{kT}} \quad (5)$$

As long as no bias voltages are applied externally, the Fermi-level, E_f , must be constant throughout the device and is generally taken as the reference level. For a complete solution, the differential equations require suitable boundary conditions. This may be provided by the fact that E_f is generally pinned near the middle of the bandgap at the GaAs surface.

However, to understand the behaviour of a structure with external voltages applied between two points (*e.g.* between an ohmic and a gate or between two quantum wells), a further condition is necessary. The external voltage sets the Fermi-level difference between the two points. A calculation of $\rho(x)$, however requires that E_f be known at every point. A third condition, in addition to the two equations 1 & 2, is necessary, because we now need to solve for three variables $(\rho(x), \psi(x), E_f(x))$ at every point.

Thermodynamically, all net particle flows in a system can be traced to a variation in the electrochemical potential [9]. The Boltzmann transport equation yields an expression relating the net particle current (\mathbf{j}) to E_f as

$$\mathbf{j} = n(x) \underline{\underline{\mu}} \nabla E_f \quad (6)$$

In the relaxation time approximation $\underline{\underline{\mu}}$ is given by

$$\underline{\underline{\mu}} = \frac{e}{4\pi^3 n} \int d^3 k \tau_e v_k v_k \frac{\partial f^0}{\partial E} \quad (7)$$

The derivative peaks sharply giving maximum weight to particles at the Fermi surface. It is easy to show that if $E(\mathbf{k})$ is spherically symmetric, then the expression reduces to the simple relation $\mu = e\tau/m^*$ at $T = 0$.

The set of equations (1-6) are used to model current flow through FETs under biasing[10], here we show that they can also be used to *approximately* model the band structure under a voltage bias between the gate and the ohmic contacts with intervening doped layers. In this case the current would correspond (physically) to the very small leakage current that flows between the gate and the conducting channels. We are not concerned with the exact magnitude of this current. However, this current must be constant, in a 1-dimensional case. Thus the variation of E_f would be slow in regions where the product of $n\mu$ is large and most of the “potential drop” would take place in regions where $n\mu$ is smaller as would be expected in analogy with voltage drops across unequal resistances in series. The assignment of a mobility

to the carriers at each point can only be done approximately, using a mobility model, rather than an evaluation of the relaxation time average, following equation 7. A “mobility-model” is an empirical relationship between the bulk-doping, electric field strength, temperature and mobility. First proposed in the context of Silicon[11], it has been adopted for use with various other semiconductors. The use of an approximate bulk mobility may seem unusual at first glance, however several other bulk parameters- like dielectric constant, effective mass and donor/acceptor ionisation energies are used in calculating the band-bending in heterostructure based devices. Also, in regions where the error from the mobility term may be the highest, it gets multiplied by a very small carrier density, thus reducing the net effect of the error on the calculation. It is also important to note that the bulk semiconductor could be in a metallic or insulating regime depending on the doping concentrations. No effort is made here to take into account the mechanisms behind the conduction process, but an empirical relation is utilised. Finally we show that the use of this approximate procedure leads to correct predictions and describes experimentally observed temperature dependent behaviour of gated structures correctly.

The specific mobility model[10, 11] used here (SIMBA) assumes that

$$\mu_{n,E0}(N_D) = \mu_{n,min} + \mu_{n,D}/[1 + (N_D/N_{n,ref})^{\alpha_n}] \quad (8)$$

$$\mu_n(\vec{E}) = \mu_{n,E0}/[1 + (\mu_{n,E0} \frac{|\vec{E}|}{\nu_{n,S}})^{\kappa_n}]^{1/\kappa_n} \quad (9)$$

$$\nu_{n,S} = \nu_{n,0} - d_{n,V}(T - T_0) \quad (10)$$

$$\mu_n(T) = \mu_n(T/T_0)^{-\gamma^n} \quad (11)$$

The empirical parameters $\mu_{n,min}=1000$ (32) $\text{cm}^2\text{V}^{-1}\text{s}^{-1}$, $\mu_{n,D} = 7200$ (400) $\text{cm}^2\text{V}^{-1}\text{s}^{-1}$, $\alpha_n=0.55$ (0.5), $N_{n,ref} = 6 \times 10^{16}$ (1.88×10^{17}) cm^{-3} $\kappa_n = 4$ (4), $\gamma^n = 1$ (2.1), $\nu_{n,0} = 1.5 \times 10^7$ (0.5×10^7) cms^{-1} , $d_{n,V} = 1.5 \times 10^4$ (1.5×10^4) $\text{cms}^{-1}\text{K}^{-1}$ and $T_0 = 300$ (300) K. The values within the braces denote the corresponding numbers for p-type material.

We have used an academic version of the software “nextnano³”[7] (developed at the Walter Schottky Institute, Munich) for solving the Poisson-Schrödinger-current equation self consistently.

A. Temperature dependence of gate action on a simple HEMT

Using the equations stated in the previous section we have calculated the carrier density at a heterointerface as a function of the surface gate voltage at various temperatures (see fig 3a). Usually the behaviour of a device with

ohmics (source and drain contacts) and a gate needs to be treated as a two-dimensional structure. We find that a simplification can be used for our purposes that allows us to model this as a one-dimensional problem. Fig 3a shows the placement of an ohmic contact at one end of the device and a surface gate on the other. The voltage bias is then applied between these two. The simplification has its limitations, but it still allows us to deduce some important conclusions while designing wafers. Experimental data from Hirakawa et al, [12] on the temperature dependence of the gate action on a HEMT structure shows certain features which a simple capacitor model of a surface gate would not explain. The calculation correctly predicts the observed features (Fig 2 of ref[12]). In particular we are able to explain the slight upward curvature of the carrier-density vs gate-voltage trace at low gate biases and high temperatures. The slight flattening of the traces at low temperatures is correctly reproduced. As far as we know, this feature of a simple gated device has not been explained clearly before. According to these calculations there is some transfer of charge to the impurity band as long as the impurity band (E_D below the conduction band in the doped AlGaAs) is in contact with the electrochemical potential. As the negative bias on the gate is increased, the conduction band and the impurity band are both pulled up and at one point moves fully above the local electrochemical potential. If the doping is higher this point would shift to more negative gate voltages. It is at this point that the gate starts acting on the 2DEG and the variation of the carrier density is fully accounted for by the gate to 2DEG capacitance. The transfer of charge into dopant states requires that there be some residual hopping-conduction in the impurity band [13]. This condition is not very difficult to satisfy (without considering tunnelling from surface states etc.), because the metal-insulator transition point in bulk-GaAs lies in the doping density range of $\sim 10^{16} - 10^{17} \text{ cm}^{-3}$.

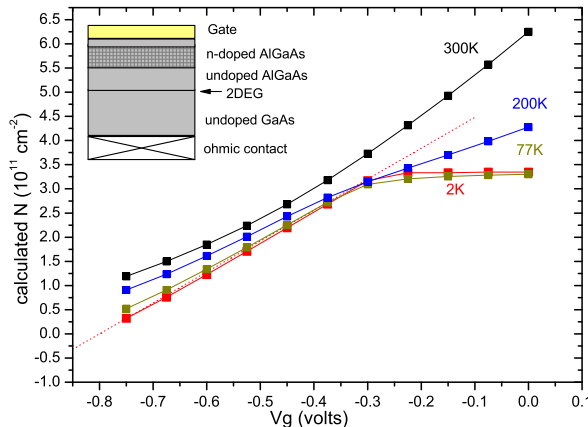


FIG. 3: (Color online) Figure shows (a) modeling of the action of a surface gate at different temperatures. The calculated traces match data from Hirakawa *et al*[12], very closely

B. Maximum doping density in inverted structures for backgate action

This procedure also allows us to estimate the maximum doping density at which a surface gate (or a backgate) would work. We use this to design an inverted hole gas that may be gated from below in a thinned sample as described in section II. An interesting observation that emerges, is that for inverted structures the doping has to be significantly less (compared to the structures described in fig 3 for a gate to work). The reason for this is that the distance of the dopants from the substrate interface in most inverted structures is much greater than the distance of the dopants from the surface in the “normal” structures. This causes the curvature of the bands, around the doped regions, in inverted structures to be much less and consequently, due to this “flatness” the dopant band cannot move away from the local electrochemical potential unless the doping itself (hence the density of dopant states) is considerably reduced.

Fig 4 shows the (simulated) effect of a bias on devices doping densities $1 \times 10^{17} \text{ cm}^{-3}$, $8 \times 10^{16} \text{ cm}^{-3}$, $5 \times 10^{16} \text{ cm}^{-3}$. The gate begins to work around a doping density of $8 \times 10^{16} \text{ cm}^{-3}$ and when the hole density is just below $2 \times 10^{11} \text{ cm}^{-2}$. The position of the impurity band with respect to the local electrochemical potential is shown in fig4. Comparison with data from measured devices show that the action of the backgate is linear in devices with a starting density of $2 \times 10^{11} \text{ cm}^{-2}$ or lower, as inferred from the calculations. However the doping density at which this happens appears to be higher (in measured devices) by nearly a factor of 2.

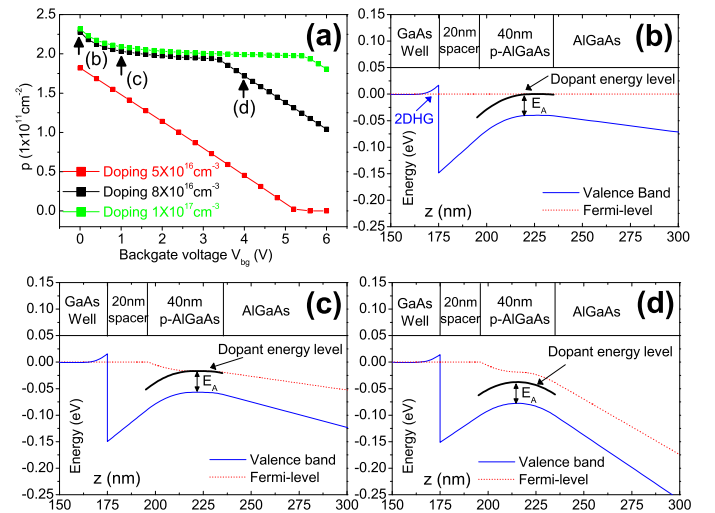


FIG. 4: (Color online) Positions of the dopant energy levels and the electrochemical potential under biasing. Figures (b),(c),(d) correspond to positions marked (b),(c),(d) with arrows in fig (a) for the $8 \times 10^{16} \text{ cm}^{-3}$ doping.

IV. FABRICATION OF AN INDEPENDENTLY CONTACTED TUNABLE ELECTRON-HOLE BILAYER

Interest in designing an electron-hole bilayer stems from the fact that the attractive Coulomb interaction between electrons and holes spaced $\sim 20\text{nm}$ apart in GaAs double quantum well (DQW) structures can give rise to novel excitonic phases[14, 15, 20]. Excitons are bosonic entities with a very low effective mass. A collection of excitons with high enough density may be expected to undergo a Bose-Einstein condensation at a much higher temperature (as high as $\sim 1\text{K}$), than a heavy inert gas or alkali atom cloud, where condensation has been observed at $\sim 200\mu\text{K}$ at the highest. However, it is now well understood that in DQW structures using the GaAs-AlGaAs system the electrochemical potential of the electrons and holes must differ by approximately 1.5V - the bandgap of GaAs. If a very closely spaced 2DHG and 2DEG are to be supported without any interlayer bias, a constant electrochemical potential would have to cut the conduction band and the valence band within 15-20nm. The necessary band bending would imply an electric field of 10^8V/m , which is far more than the breakdown field of GaAs. However to bias a layer with respect to another layer, one needs independent ohmic contacts to both layers. Additionally the narrow interlayer barrier must be able to withstand the bias with very little leakage. Though excitonic phases in these structures have been predicted many years back[15], but experimentally such devices have proved extremely difficult to make. Even with the present day developments of MBE techniques, these devices appear to be on the borderline of feasibility. However the possibility of excitons with infinite lifetime, leading to phenomena like dipolar superfluidity, BEC etc have led to quite a few experimental attempts in recent years[16-19]. Here we apply the backgating technique presented in section I, to design a bilayer device in which the two layers are independently contacted. The two densities can be tuned independently, within limits, by using a backgate and an interlayer voltage. Here we present data from three devices.

In device A and B (see fig 5 for a schematic) an inverted hole gas was created by modulation doping (Carbon in AlGaAs) using the estimates presented in the previous section. Device C was completely undoped and the hole gas was created by biasing the backgate to attract holes below the contacts. Considering the dielectric constant of GaAs, $\epsilon/\epsilon_0 \approx 12.8$, a gate $50-60\mu\text{m}$ away from the quantum well is expected to be able to change (either deplete or induce) carrier densities by $\approx 6 \times 10^{10}\text{cm}^{-2}$ for every 50 volts of biasing. The measured changes in the carrier densities were close to this expected number. For example in the data from device A (see fig 6), the hole density changes by $\Delta p \approx 2 \times 10^{11}\text{cm}^{-2}$ for a backgate bias of 150V. AuBe contacts alloyed at 500°C were used to contact the 2DHG. In device C (fully undoped), the backgate has two discontinuous parts. The part below the

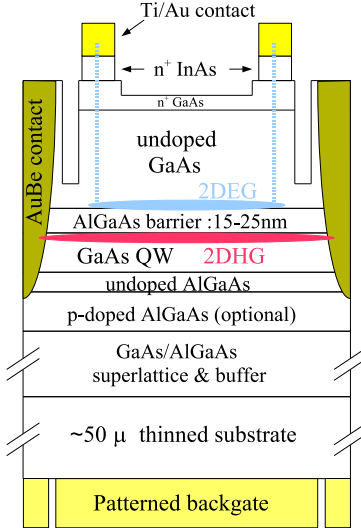


FIG. 5: (Color online) Generalised schematic of the electron-hole devices. Certain details like the doping levels, width of the quantum wells, width and composition of the barriers vary between devices. See table 1 for these details

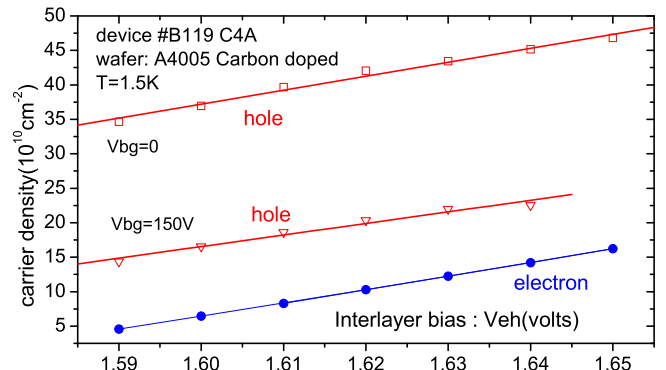


FIG. 6: (Color online) Action of backgate. Data from device A. The electron and hole densities were not matched in this device. The electron densities are shown for $V_{bg}=0$. The change in the electron density with backgate voltage is very small.

p-type contacts is biased negative to attract holes, the part below the central region (which overlaps the 2DEG), is usually biased positively to deplete excess holes. There is a $20\mu\text{m}$ gap between the two gates (see fig 1). Contact to the overlapping 2DEG was made by using a different technique[16]. The top layer of the wafer consisted of n^+ InAs ($8 \times 10^{18}\text{cm}^{-3}$ Si doping). The surface states of InAs have the unusual property of pinning the Fermi level *above* the bottom of the conduction band and not at the midgap like the surface states of GaAs. Thus any metal deposited on a clean InAs surface would not see a barrier for electron injection. It can be interpreted as a negative

Schottky barrier and does not require any post deposition annealing. Using a selective etch (dry conc. HCl) the InAs is removed from all places except where contacts to the electron layer are required. Since this contacting process requires no annealing, the contact material does not spike into the underlying semiconductor and is able to form a low resistance shallow contact to the 2DEG, without shorting to the 2DHG.

TABLE I: Summary of the three devices. All the three devices have an approximately $1\mu\text{m}$ thick GaAs/AlGaAs superlattice near the substrate.

device	p-doping	QW width	barrier	matched densities possible
A	$1.5 \times 10^{17}\text{cm}^{-3}$ $\times 40\text{nm}$ wafer ID A4005	40nm	25nm Al _{0.3} Ga _{0.7} As	No
B	$5 \times 10^{16}\text{cm}^{-3}$ $\times 40\text{nm}$ wafer ID A4170	20nm	15nm Al _{0.9} Ga _{0.1} As	Yes
C	no doping wafer ID A4142	20nm	25nm Al _{0.3} Ga _{0.7} As	Yes

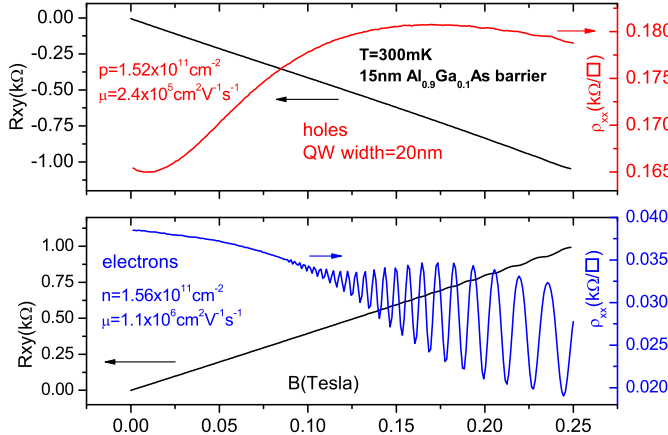


FIG. 7: (Color online) Data from device B, $n=p=1.5 \times 10^{11}\text{cm}^{-2}$

A typical variation of the electron and hole densities with the interlayer bias (V_{eh}) and the backgate bias (V_{bg}) is shown in fig 6. The comparatively higher doping in this device led to a higher hole density.

Comparing the electron and hole mobilities in the undoped device (C) at $n = p = 7 \times 10^{10}\text{cm}^{-2}$ we find that $\mu_e/\mu_h = 3.2$. Assuming an effective mass ratio $m_h^*/m_e^* \approx$

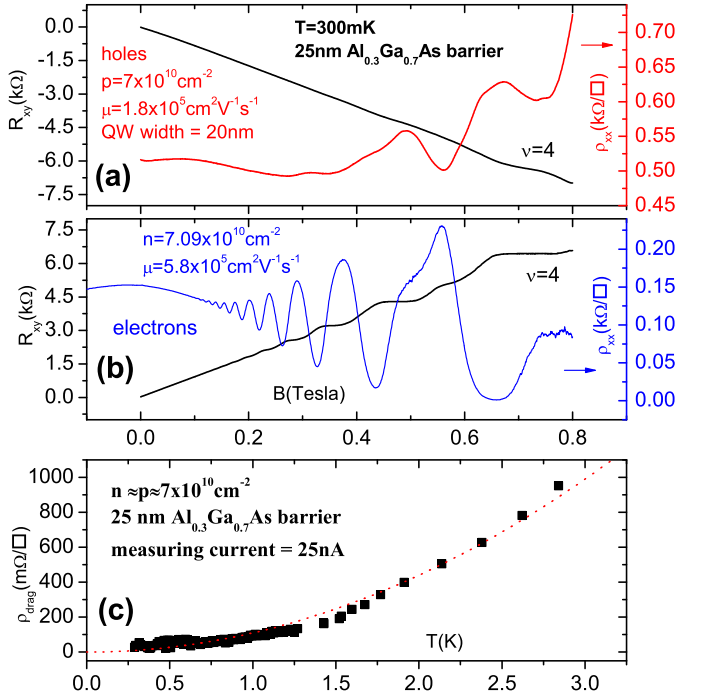


FIG. 8: (Color online) (a) & (b): Data from device C, $n=p=7 \times 10^{10}\text{cm}^{-2}$. The lowest panel (c) shows drag resistivity measured by passing current through the hole layer and measuring the voltage across the electron layer.

7.5, (appropriate for heavy holes at low densities) we find that the transport scattering times $\tau_h/\tau_e \approx 2$. This probably results from the doped surface contributing to scattering in the electron layer more than it does to the hole layer. In addition hole wavefunctions tend to be smaller than electrons, leading to an overlap with a smaller number of background impurity sites. Both the 2DEG and the 2DHG otherwise sees a similar background impurity density. A comparison of the mobilities in device C at $n = p = 1.5 \times 10^{11}\text{cm}^{-2}$ gives $\mu_e/\mu_h = 4.6$. Calculations of E_{hole} vs $k_{||}$ for the holes using $\vec{k} \cdot \vec{p}$ method show no significant non-parabolicity or mixing of light and heavy holes at densities less than $p = 2 \times 10^{11}\text{cm}^{-2}$ for a 20nm QW[21]. These calculations are not presented here but we continue to assume a parabolic heavy hole band for these estimates and find that $\tau_h > \tau_e$, though the difference appears to decrease at higher densities[22].

In these devices, we are also able to directly measure the interlayer interaction by the Coulomb drag method[23]. These measurements have been performed on some of the devices at temperatures down to 300mK but have not yet shown unambiguous signatures of an excitonic phase. However regimes of stronger electron-hole interaction can be achieved in these devices, by reducing the densities and the barrier width further. It is expected that these devices would prove useful in transport based studies of bilayer excitonic phases.

V. CONCLUSION

In conclusion, we have developed a method to achieve the functionality of a double-sided mask aligner using a much less expensive and more commonly available single-sided aligner. We have used this technique in conjunction with a numerical procedure to estimate the behaviour of the electrochemical potential in doped and (back)gated devices under biasing, to design an electron-hole bilayer with independent contacts and a patterned backgate. In these systems, the interlayer scattering rate between electrons and holes is of considerable interest. The scattering

rate may show some very interesting characteristics at low temperatures and densities. Our alignment method and calculation procedure are however applicable to a much wider variety of semiconductor devices.

VI. ACKNOWLEDGEMENTS

This work was funded by EPSRC, UK. IF would like to thank Toshiba Research Europe Ltd. for financial support. MT acknowledges support from the Gates Cambridge Trust.

-
- [1] T.J. Gramilla, J.P. Eisenstein, A.H. MacDonald, L.N. Pfeiffer and K.W. West, *Physical Review Letters* **66**, 1216 (1991), N. Hill, et al., *Physical Review Letters* **78**, 2204 (1997)
 - [2] A. Kurobe, I. M. Castleton, E. H. Linfield, M. P. Grimshaw, K. M. Brown, D.A. Ritchie, M. Pepper and G.A.C. Jones, *Physical Review B* **50**, 4889 (1994), H. W. Jiang and E. Yablonovitch *Physical Review B* **64**, 041307 (2001)
 - [3] R. Crook, A.C. Graham, C.G. Smith, I. Farrer, H.E. Beere and D.A. Ritchie, *Nature*, **424**, 751 (2003)
 - [4] A. Kawaharazuka, T. Saku, Y. Hirayama and Y. Horikoshi, *Journal of Applied Physics* **87**, 952 (2000)
 - [5] E.W. Linfield, G.A.C. Jones, D.A. Ritchie and J.H. Thompson *Semiconductor Science and Technology* **8** 415 (1993)
 - [6] M.V. Weckwerth, J.A. Simmons, N.E. Harff, M.E. Sherwin, M.A. Blount, W.E. Baca, H.C. Chui, *Superlattices and Microstructures* **20**, 561 (1996)
 - [7] Nextnano³ device simulation package; see <http://www.nextnano.de>
 - [8] F. Stern and W. E. Howard, *Physical Review* **163**, 816 (1967). A calculation tool is available from <<http://www.nd.edu/gsnider/>>
 - [9] A. Marshak and C. Van Vliet, *Journal of Applied Physics*, **81**, 10 (1997)
 - [10] Kidong Kim, Ohseob Kwon, Jihyun Seo and Taeyoung Won, *Japanese Journal of Applied Physics* **43**, No. 6B, 37843789 (2004)
 - [11] D. M. Caughey and R. E. Thomas, *Proc IEEE* **55**, 2192 (1967)
 - [12] K. Hirakawa and H. Sakaki, em *Physical Review B* **33**, 8291 (1986)
 - [13] N. F. Mott and W. D. Twose, *Advanced Physics* **10**, 107 (1960)
 - [14] P. B. Littlewood and Xuejun Zhu, *Physica Scripta* **T68**, 56 ,(1996)
 - [15] Y. E. Yudson and V. I. Yudson, *Soviet Physics J.E.T.P.* **44**, 389 (1976)
 - [16] J. A. Keogh, K. Das Gupta, H.E. Beere, D.A. Ritchie and M. Pepper., *Applied Physics Letters* **87**, 202104 (2005)
 - [17] J. A. Seamons, D. R. Tibett, J. L. Reno, and M. P. Lilly, *Applied Physics Letters* **90**, 052103 (2007)
 - [18] U. Sivan, P. M. Solomon and H Shtrikman, *Physical Review Letters* **68**, 1196 (1992)
 - [19] M. Pohlt, M. Lynass, J. G. S. Lok, W. Dietsche, K. v. Klitzing, K. Eberl and R. Mühle, *Applied Physics Letters* **80**, 2105 (2002)
 - [20] G. Vignale and A. H. McDonald, *Physical Review Letters* **76**, 2786 (1996)
 - [21] R. Winkler, *Spin-Orbit Coupling Effects in Two-Dimensional Electron and Hole Sysytems*, Springer Tracts in Modern Physics, Berlin (2003).
 - [22] During the preparation of this manuscript, we found that a more detailed analysis of this point has been very recently presented. C.P. Morath *et al* condmat arXiv 0803.1402
 - [23] M.B. Pogrebinsky, *Soviet Phys. Semiconductors.*, **11**, 372 (1977), P.J. Price, *Physica* **117B**, 750 (1983)